Check for updates

Hydrogen desorption from the surface and subsurface of cobalt†

Ryan A. Ciufo, [ID] [ab] Sungmin Han,[a] Michael E. Floto, [ID] [a] J. Ehren Eichler,[a]
Graeme Henkelman [ID] ★[ab] and C. Buddie Mullins [ID] ★[ac]

The influence of coverage on the diffusion of hydrogen into the subsurface of cobalt was studied using density functional theory (DFT) and temperature programmed desorption (TPD). DFT calculations show that as the hydrogen coverage on Co(0001) increases, the barrier for hydrogen diffusion into the bulk decreases by 20%. Additionally, subsurface hydrogen on a hydrogen covered surface was found to be more stable when compared to a clean cobalt surface. To test these theoretical findings experimentally, excited hydrogen was used in an ultra-high vacuum environment to access higher hydrogen coverages. Our TPD studies showed that at high hydrogen coverages, a sharp low temperature feature appeared, indicating the stabilization of subsurface hydrogen. Further DFT calculations indicate that this sharp low temperature feature results from associative hydrogen desorption from a hydrogen saturated surface with a population of subsurface hydrogen. Microkinetic modelling was used to model the TPD spectra for hydrogen desporption from cobalt with and without subsurface hydrogen, showing reasonable agreement with experiment.

1 Introduction

A fundamental understanding of the interaction of hydrogen with metal surfaces is of great interest for a number of fields ranging from fundamental surface science to materials science to engineering.[1–3] The desire for this understanding comes from the decisive role that hydrogen typically plays in a number of reactions and processes. For example, hydrogen–metal interactions are of particular importance in the field of Fischer–Tropsch catalysis, where there has been debate about the specific role of hydrogen. A number of papers argue that hydrogen influences the dissociation of carbon dioxide, while others argue that hydrogen acts as a spectator to the rate determining step.[4–6] There have been several theoretical and experimental studies focused on the adsorption of hydrogen to well defined cobalt model surfaces with the aim of better understanding the role of hydrogen in different processes.

Of particular interest are the studies looking at hydrogen adsorption to Co(poly), Co(0001), and corrugated Co(10$\bar{1}$0) in

vacuum. Co(poly) is a good model catalyst to represent multi-faceted high-surface area catalysts, while the (0001) and (10$\bar{1}$0) facets are the lowest energy Co hcp surfaces.[7] On hcp cobalt surfaces, two key hydrogen desorption features are typically observed. On Co(10$\bar{1}$0), temperature programmed desorption (TPD) shows two desorption features at $\sim$275 K (β_1) and between 325–350 K (β_2).[8] Notably, the β_1 feature on Co(10$\bar{1}$0) shows a sharp desorption characteristic that has been attributed to surface reconstruction, while the β_2 feature is attributed to recombinative desorption of hydrogen. Similarly, Co(0001) and Co(poly) show a β_2 feature appearing between 350–400 K, and a β_1 feature appearing anywhere from 200–350 K.[9–12] The β_2 feature has been shown to be associative H_2 desorption, but there has been debate on the nature of the β_1 feature. While some claim that the β_1 feature is attributed to atomic hydrogen bound to surface defect sites,[10] others claim that defects should produce more strongly bound hydrogen which would desorb at higher temperatures.[9] Lisowski and Christmann have both suggested the possibility of the contribution of subsurface hydrogen to the β_1 feature.[9,13,14] The claim of subsurface hydrogen holds some credibility, since Ni (which is a periodic neighbor of Co) has been shown to stabilize subsurface hydrogen under ultra-high vacuum (UHV).[15–17] Additionally, desorption peaks resultant from subsurface hydrogen have been seen on other model catalysts, such as palladium surfaces.[18–21] More interestingly, at higher pressures (near 1 atm), there have been reports of hydrogen embrittlement of cobalt and cobalt alloys, which would require hydrogen penetration into the subsurface.[22] These

[a] *Department of Chemistry, University of Texas at Austin, Austin, Texas 78712, USA. E-mail: mullins@che.utexas.edu*
[b] *The Oden Institute for Computational Engineering and Science, University of Texas at Austin, Austin, Texas 78712, USA*
[c] *The McKetta Department of Chemical Engineering, Texas Materials Institute, Center for Electrochemistry, University of Texas at Austin, Austin, Texas 78712, USA. E-mail: henkelman@utexas.edu*
† Electronic supplementary information (ESI) available. See DOI: 10.1039/d0cp02410d

This journal is © the Owner Societies 2020

Phys. Chem. Chem. Phys., 2020, **22**, 15281–15287 | **15281**

findings show that a better understanding of hydrogen adsorption and diffusion on and in cobalt surfaces is needed to bridge the gap between high and low pressure regimes.

Along with the above experimental studies, a few theoretical studies have been performed to investigate the nature of subsurface hydrogen on cobalt surfaces. Klinke and Broadbelt performed non-spin polarized density functional theory (DFT) calculations on hydrogen on Co(0001).[23] They saw that while unfavorable, subsurface sites were more stable than hydrogen bound to top sites. Additionally, Klinke and Broadbelt claimed that hydrogen adsorption is not coverage dependent, which was later disproven by van Helden *et al.*[10] Greeley and Mavrikakis performed similar studies with spin polarization and zero-point energy corrections. Their calculations also showed an unfavorability of hydrogen in the subsurface, however both of these studies looked only at low coverage of hydrogen on cobalt.[24] Based on these past findings, we aimed to study the coverage dependence of subsurface hydrogen on cobalt using computational and experimental ultra-high vacuum techniques.

2 Experimental

2.1 Computational details

We performed spin-polarized DFT calculations using the Vienna ab initio Simulation Package (VASP).[25–28] The projector augmented wave framework was used to treat interactions between the core and valence electrons.[29,30] Electronic exchange and correlation were described with the generalized gradient approximation – Perdew–Burke–Ernzhof (PBE) functional.[31,32] The systems were modelled as 4-layer slabs with a 2×2 supercell. The bottom two layers were fixed in their bulk positions, and the top two layers were allowed to relax freely. A 10 Å vacuum layer was added above and below the slabs to provide separation. Optimized lattice parameters of $a = 2.49$ Å and $c = 4.03$ Å were determined and are in agreement with experimental values of 2.50 Å and 4.06 Å, respectively.[33] A cut-off energy of 450 eV was used for all calculations. The Brillouin zone was sampled with a $9 \times 9 \times 1$ mesh using the Monkhorst–Pack scheme.[34] Methfessel-Paxton[35] smearing was employed with a width of 0.2 eV. The convergence criteria for the electronic structure and atomic geometry were set to 10^{-5} eV and 0.001 eV Å^{-1}, respectively. All transition states and energy barriers were calculated using the climbing image nudged elastic band (Cl-NEB) method,[36] where five intermediate images were generated between the initial and final states. The adsorption binding energies (BEs) were calculated with respect to the relaxed clean slab (E_{slab}) and an isolated hydrogen molecule (E_{H_2}):

$$ BE = \frac{1}{x}\left[E_{slab+xH} - E_{slab} - \frac{x}{2}E_{H_2} \right] \quad (1) $$

With x being the number of hydrogen atoms in the unit cell. To account for coverage effects on binding energy, we sequentially introduced additional hydrogen atoms to the unit cell. Three-fold hollow sites were found to be the most stable for hydrogen binding, with fcc sites being slightly more stable (-0.52 eV for fcc *vs.* -0.48 eV for hcp). Convergence tests were performed by increasing the energy cut-off, force criterion, and number of layers in the slab model. No significant changes in the binding energies and barriers (≤ 0.005 eV) or the optimized structures were found.

Microkinetic analysis was used to simulate TPD spectra. The rate of hydrogen desorption was expressed using the Arrhenius expression:

$$ r = -\frac{d\theta}{dt} = \theta^n \nu e^{\left(\frac{-E_d}{k_b T}\right)} \quad (2) $$

where θ is the coverage of adsorbed species, n is the order of the desorption process, ν is the vibrational prefactor, and E_d is the desorption energy.[37] For all cases, ν was assumed to be 10^{13} s^{-1}. For associative hydrogen desorption, coverage dependent DFT calculated desorption energies were used based off of a linear fit (Fig. S1, ESI†). For examples involving subsurface hydrogen, a second desorption energy relating to the associative desorption of hydrogen from above a subsurface hydrogen was used. After the associative desorption of two surface hydrogen, subsurface hydrogen then repopulates the vacant surface sites.

2.2 Experimental details

To study the interactions of hydrogen on a cobalt surface and diffusion into the subsurface, we performed TPD studies under UHV conditions. All experiments were performed in a UHV molecular beam surface scattering system with a base pressure of 1.0×10^{-10} Torr, which has been described previously.[38] In brief, the apparatus is capable of generating two separate molecular beams, and is equipped with an Extrel C-50 quadrupole mass spectrometer, a Bruker Tensor 27 Fourier transform infrared spectrometer with a mercury-cadmium telluride detector, and a Physical Electronics 10-500 Auger electron spectrometer (AES). A rectangular polycrystalline cobalt sample (Goodfellow 99.9%) (15 mm × 10 mm × 1 mm) is held in vacuum by spot welded cobalt wires attached to a liquid nitrogen reservoir to both cool and resistively heat the sample. The sample temperature was monitored by a K-type thermocouple spot welded to the back of the sample. The cobalt sample was cleaned with Ar$^+$ sputtering (2000 V accelerating voltage) followed by annealing to 950 K for 30 seconds. AES was performed to confirm the cleanliness of the sample.

Hydrogen dosing experiments were performed by backfilling hydrogen with the clean Co(poly) sample held at 100 K. For cases using excited hydrogen, hydrogen was backfilled through a tungsten capillary which was heated *via* electron bombardment (20 mA emission current). Following hydrogen exposure, samples were resistively heated at 5 K s^{-1} to desorb adsorbed species.

3 Results and discussion

Past computational work by Klinke and Broadbelt, and Greeley and Mavrikakis studied subsurface hydrogen on Co(0001).[23,24] However, their work only considered low coverages of hydrogen ($\theta = 0.25$). To expand upon this work, we calculated binding

15282 | *Phys. Chem. Chem. Phys.*, 2020, **22**, 15281–15287

This journal is © the Owner Societies 2020

energies and diffusion barriers for subsurface H when the surface coverage of H was $\theta = 1.0$ (1 H per surface Co). Our motivation for studying a hydrogen saturated surface comes from past experimental work by Johnson and coworkers which showed subsurface hydrogen on Ni(111) at high hydrogen coverages.[15–17] To this end, we calculated the transition of a single H atom from a surface fcc site to a subsurface octahedral site on a Co(0001) surface both with no additional H ($\theta = 0.25$) present and on a H saturated Co(0001) surface ($\theta = 1.0$). As seen in Fig. 1a, a barrier of 0.97 eV is found for the transition from a surface fcc site to a subsurface octahedral site. The octahedral site has a binding energy 0.76 eV higher than the surface site, which is 0.24 eV above reference energy level ($1/2E_{H_2} + E_{slab}$), showing the endothermic nature of the subsurface site. This agrees well with previous work by Greeley and Mavrikakis.[24] It was also found that the barrier for hydrogen resurfacing is 0.21 eV. Lastly, only a slight perturbation of the Co surface was observed, with a Co atom above a subsurface hydrogen rising out of the lattice by only 0.04 Å (in the z direction). This is significantly less than the perturbation seen for subsurface hydrogen on Ni(111) (where a Ni atom lifts out of the surface

by 0.25 Å), suggesting that subsurface hydrogen in cobalt does not induce significant structural change.[39]

When looking at diffusion into the subsurface on a hydrogen covered surface (Fig. 1b), it can be seen that the barrier for diffusion is 0.77 eV, which is 0.2 eV lower when compared to Fig. 1a ($\theta = 0.25$). The binding energy of the subsurface hydrogen is found to be approximately 0.13 eV for the hydrogen covered surface as compared to 0.24 eV for $\theta = 0.25$, showing a decreased endothermicity of the octahedral site. Lastly, the barrier for resurfacing of the subsurface hydrogen on the hydrogen covered surface is slightly higher than for the $\theta = 0.25$ case (0.22 vs. 0.21 eV). These calculations show that while endothermic, diffusion of hydrogen into the subsurface and subsequent stabilization are possible, and more so for hydrogen saturated surfaces.

To study the interaction of hydrogen on our sample, we held our sample at 100 K and exposed the surface to various coverages of hydrogen. The sample was then heated to 900 K at a rate of 5 K s^{-1} to study H desorption from the surface (Fig. 2). At low coverages (Fig. 2, grey curve), it is seen that hydrogen produces a single desorption feature (β_2) at 350 K. As the exposure of H$_2$ is increased, this feature increases in size and shifts to lower temperatures (Fig. 2, yellow curve). As exposure is increased again, a second desorption feature (β_1) begins to appear at ~ 215 K. These two features then reach a maximum intensity between 5 L and 100 L, with no increase in desorption signal observed above 100 L. At saturation coverages (Fig. 2, red and black curve), the β_1 feature peaks at ~ 215 K and the β_2 feature peaks at ~ 305 K. Using Redhead analysis,[37] we observe a difference in binding energy between the β_1 and β_2 features on a saturated surface of 0.22 eV.

As mentioned above, similar desorption patterns have been observed previously for polycrystalline cobalt and cobalt (0001).[9–11,13,14] The β_2 feature, which shows second order character (decreasing T_{max} with increasing coverage) has been attributed to associative desorption of H$_2$ from the surface. However, there has been some debate regarding the nature of
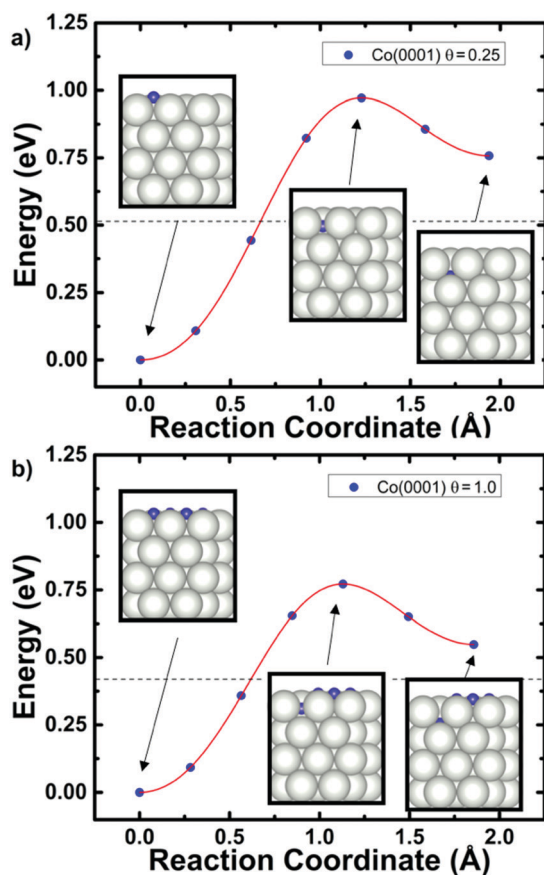

Fig. 1 CI-NEB of diffusion of a single hydrogen from a surface fcc site to a subsurface octahedral site on (a) clean ($\theta = 0.25$) and (b) hydrogen covered surface ($\theta = 1.0$). The insets show the initial, saddle and final states. White spheres are cobalt, blue are hydrogen and the dashed line represents the reference energy level of a clean surface and H$_2$ in the gas phase.
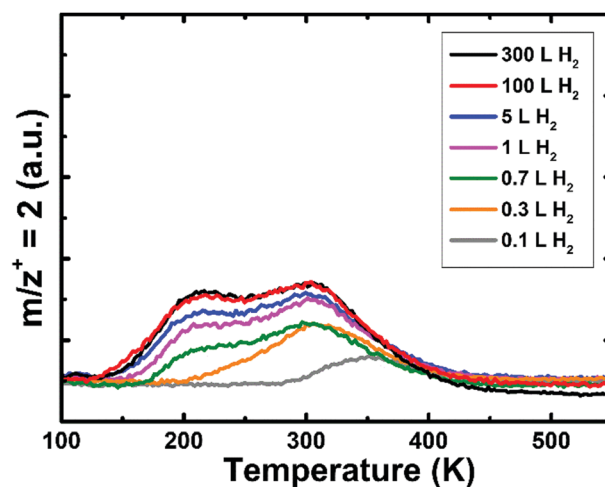

Fig. 2 TPD after various exposures of hydrogen with the sample held at 100 K.

the β_1 feature, which appears to follow a first order desorption mechanism (T_{max} remains constant with increasing coverage). Lisowski suggested that the β_1 feature is comprised of two distinct features on polycrystalline cobalt films.[13,14] Of these two peaks, the lower temperature region within the β_1 feature was attributed to hydrogen incorporation into the subsurface, and the higher temperature feature attributed to defect sites. Christmann observed a similar β_1 feature on Co(0001), and was able to approximate a desorption energy based on a first order Redhead analysis, but was unable to do further analysis due to the interference from the β_2 feature. In contrast, Westrate *et al.* saw that the β_1 feature appeared almost exclusively on defect rich Co(0001) surfaces.[10] Lastly, the small shoulder seen near 125 K was previously attributed to molecularly adsorbed hydrogen (most likely at defect sites).[13,40] Based upon this previous research, the β_1 feature seen in Fig. 2 is most likely associative desorption of atomic hydrogen from surface defects, which are innately present in our polycrystalline sample. Additionally, as shown by Westrate *et al.*,[10] the presence of defects can shift the the β_2 feature to lower temperatures as compared to pristine Co(0001) – this is likely observed in the β_2 feature seen in Fig. 2.

To access higher coverages of hydrogen under UHV conditions and better simulate industrially relevant pressure regimes, it is possible to use excited (vibrationally or kinetically) molecules or atomic gasses.[15–17] To this end, we produced excited hydrogen by backfilling through a tungsten capillary which was heated by electron bombardment (20 mA emission current).[41–43] Exciting the hydrogen in this manner likely produces a mixture of atomic hydrogen and exposure to this excited hydrogen should have two effects. First, higher coverages of hydrogen should be obtainable, which our calculations show relate to lower diffusion barriers into the subsurface. Secondly, the high energy of the excited hydrogen atoms/molecules can assist in overcoming the barriers to subsurface diffusion. TPD measurements were performed following exposure to various coverages of excited hydrogen. As seen in Fig. 3, TPD after an exposure of 5 L of excited hydrogen (grey curve) produces a feature of similar shape and magnitude as 5 L of unexcited hydrogen (Fig. 2, purple curve). However, as exposure is increased up to 500 L, it is seen that the β_1 and β_2 features continues to grow in (as compared to with unexcited hydrogen), suggesting increased surface coverage of adsorbed dissociated hydrogen. This finding is unsurprising, given that past studies of hydrogen on cobalt surfaces show that under ultra-high vacuum conditions, typical saturation levels of H_2 can be less than $\theta = 0.75$.[10,44] This is also consistent with previous work with excited hydrogen.[15–17] When the exposure of excited H_2 is further increased to 1000 L and 1500 L, a sharp feature begins to grow in at 190 K (compared to 215 K for unexcited hydrogen), while the β_2 feature remains unchanged. This new feature at 190 K will be denoted as β_{1s} to simplify our discussion. Additionally, the β_2 feature shifts to a lower temperature ($\sim$250 K) as compared to the saturated β_2 seen with unexcited hydrogen (Fig. 2, $\sim$305 K). This is consistent with the second order nature of associative hydrogen desorption and the coverage dependent binding energy of hydrogen on cobalt.[9,10]
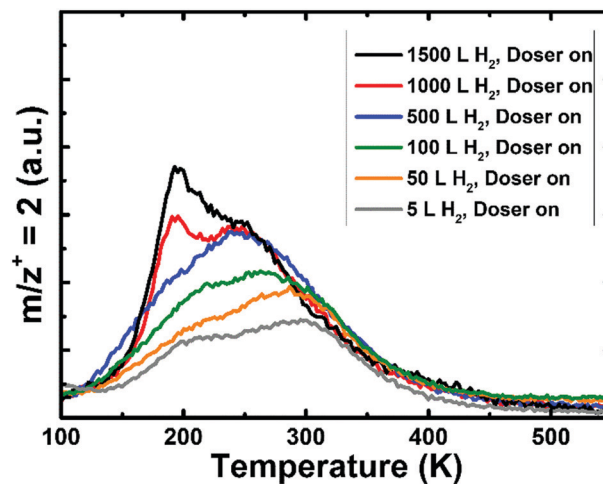

Fig. 3 TPD after various exposures of excited hydrogen with the sample held at 100 K.

Lastly, the new low temperature feature at 190 K again appears to follow a first order process, with T_{max} remaining constant with increasing coverage from 1000 to 1500 L.

Since this new β_{1s} feature is continually increasing while the β_2 feature is saturated, this suggests that new sites are being accessed at these high coverages, which are likely subsurface sites. A similar desorption feature (sharp, low temperature, first order characteristic) was seen by Johnson *et al.* for subsurface hydrogen on Ni(111).[15–17] Additionally, similar features are seen for subsurface hydrogen on palladium surfaces.[18–21] Notedly, the similarity of the line shape in Fig. 3 to the work by Ernst *et al.* could also suggest surface reconstruction.[8] However, the barrier to restructuring found by Ernst *et al.* was on the order of 2.5 kJ mol^{-1}, and therefore should have been observed without excited hydrogen. Additionally, hydrogen desorption and concurrent lifting of the reconstruction is expected to occur at temperatures higher than seen for our β_{1s} feature ($\sim$275 K for lifting *vs.* 190 K observed in Fig. 3). From this, we conclude that the sharp β_{1s} feature seen at 190 K in Fig. 3 (red and black curves) is resultant from the presence of subsurface hydrogen. Lastly, from a Redhead analysis[37] of the TPD after exposure to 1500 L of excited hydrogen (Fig. 3, black curve), the desorption energy for the feature seen near $\sim$190 K (β_{1s}) is 0.13 eV lower than the desorption energy for associative hydrogen desorption ($\sim$250 K, β_2).

When looking at the TPD spectra following exposure to excited hydrogen (Fig. 3), it is interesting that from 500 L to 1000 L, the area under the desorption curve increases by only approximately 1%. However, from 1000 L to 1500 L, the area under the desorption curve increases by $\sim$13%. The similarity in area of the 500 L and 1000 L curves suggests the coverage that correlates to the formation of subsurface hydrogen occurs between these two exposures. Then, as coverage is increased, subsurface hydrogen becomes stabilized. That is to say, the 190 K feature does not begin to appear until after the β_1 and β_2 features (and therefore the surface) saturate. Additionally, since no sharp feature at 190 K is seen for low hydrogen exposures,

15284 | *Phys. Chem. Chem. Phys.*, 2020, **22**, 15281–15287

This journal is © the Owner Societies 2020

we conclude that hydrogen exposure and coverage (and not necessarily the high energy of the excited hydrogen molecules) are necessary for stabilization of subsurface hydrogen. While the excited nature of the hydrogen may help hydrogen to overcome the large barrier to diffusion, the higher coverages resultant from the excited hydrogen help to stabilize hydrogen in the subsurface. This can be better seen when looking at the similarity of the 5 L excited hydrogen exposure TPD (Fig. 3, grey curve) to the line shape of the TPD following saturation with unexcited hydrogen (Fig. 2, black curve). Both curves show a similar quantity of desorption (and therefore similar surface coverage of hydrogen). This shows that at similar hydrogen coverages, excited hydrogen behaves similarly to unexcited hydrogen.

To better understand the low temperature desorption process and gain insight into the desorption mechanism, additional DFT calculations were performed on a number of hydrogen desorption processes from Co(0001). We calculated the desorption energy for various processes involving surface and subsurface hydrogen and compared them to the desorption energy for associative desorption from a hydrogen saturated surface (Table 1, $\theta = 1.0$, $\theta_{subsurface} = 0.0$). The process that best fit the energy difference between the β_{1s} feature at 190 K and the β_2 feature at 250 K was the associative desorption of two surface hydrogen atoms from a hydrogen covered Co(0001) surface that had 25% subsurface hydrogen ($\theta = 1.0$, $\theta_{subsurface} = 0.25$). This desorption process is illustrated in Fig. 4. The calculated difference between hydrogen desorption from a saturated surface ($\theta = 1.0$, $\theta_{subsurface} = 0.0$) and a saturated surface with 25% subsurface hydrogen ($\theta = 1.0$, $\theta_{subsurface} = 0.25$) was found to be 0.12 eV. This compares well to the 0.13 eV energy difference found between the β_{1s} feature and β_2 feature for 1500 L of excited hydrogen (Fig. 3, black curve) using Redhead analysis.[37]

Using the coverage dependent desorption energies calculated from DFT (Table 1), we simulated TPD for hydrogen on Co(0001) (Fig. 5). The simulated desorption spectra show one feature for coverages up to $\theta = 1.0$, $\theta_{subsurface} = 0.0$, which differs from the TPD spectra in Fig. 2. This is most likely resultant from the lack of defects in the Co(0001) model. As discussed above and in detail by others, defects appear to be the predominant cause of the β_1 feature seen with unexcited hydrogen.[10] Once subsurface hydrogen are included in the simulation ($\theta = 1.0$, $\theta_{subsurface} = 0.25$), a sharp low temperature
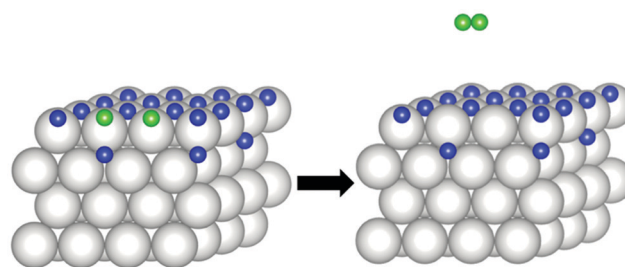

Fig. 4 Depiction of possible desorption mechanism where two surface hydrogen (green balls) desorb from two fcc sites with a subsurface hydrogen atom in an oct site ($\theta = 1.0$, $\theta_{subsurface} = 0.25$). White = cobalt, blue = hydrogen, green = hydrogen.
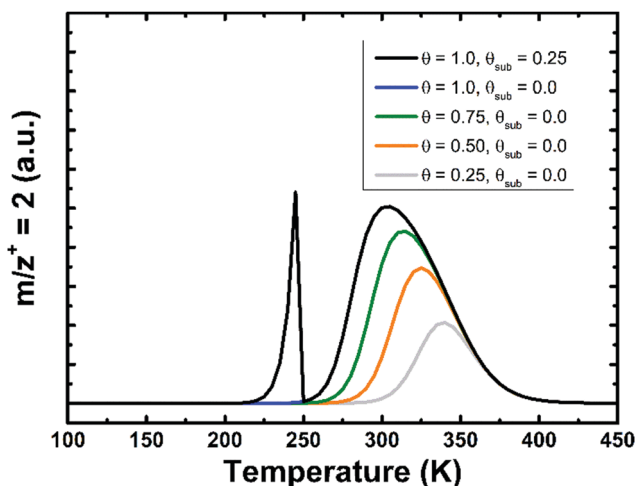

Fig. 5 Simulated TPD spectra for hydrogen on Co(0001). Note: the black and blue features overlap above 250 K.

feature appears (β_{1s}). The temperature difference between the two peaks for the case of a hydrogen covered surface with subsurface hydrogen ($\theta = 1.0$, $\theta_{subsurface} = 0.25$) is 57 K, which aligns well with the experimental temperature difference of 52 K observed in Fig. 3 (black curve) for excited hydrogen. The overall shift in the simulated spectra to higher desorption temperatures is most likely resultant from not including zero-point energy corrections (which should decrease binding energies by ~0.1 eV) and the tendency of the PBE functional to overestimate chemisorption energies.[45] The agreement between the simulated TPD and TPD following exposure to excited hydrogen show that our suggested mechanism of desorption of hydrogen from above subsurface hydrogen is a likely contributor to the experimentally observed β_{1s} feature.

4 Conclusions

In conclusion, we show that high coverages of hydrogen increase the rate of hydrogen diffusion into the subsurface of cobalt. Calculations show that having a hydrogen saturated surface ($\theta = 1.0$) decreases the subsurface diffusion barrier from

Table 1 Calculated desorption energies per H_2 molecule at various coverages (θ) on Co(0001) vibrationally excited molecular hydrogen

Hydrogen coverage, θ, $\theta_{subsurface}$ (ML)	Desorption energy[a] (eV per H_2)
0.25, 0.0	1.03
0.5, 0.0	1.00
0.75, 0.0	0.97
1.0, 0.0	0.94
1.0, 0.25	0.82

[a] Desorption energy is calculated as $-2BE$, where BE is defined as the binding of atomic hydrogen referenced to gas phase H_2 and a clean cobalt slab at infinite separation.

0.97 to 0.77 eV while also decreasing the endothermicity of subsurface hydrogen from 0.24 to 0.13 eV. These calculations were supported by UHV adsorption experiments where excited hydrogen was used to increase hydrogen coverage. TPD experiments after excited hydrogen exposure showed a sharp low-temperature feature which is associated with subsurface hydrogen. This sharp low temperature feature was only seen once surface saturation occurred, and was not seen at low exposures of excited hydrogen. Further DFT calculations suggest that this feature is the result of associative hydrogen desorption from a hydrogen saturated surface with a population of subsurface hydrogen (θ = 1.0, $\theta_{subsurface}$ = 0.25). Using the coverage dependent desorption energies for hydrogen on Co(0001) and the desorption energy of hydrogen from a hydrogen saturated surface with subsurface hydrogen, we simulated TPD spectra which resembles the experimental TPD following exposure to excited hydrogen. These findings show that hydrogen coverage promotes hydrogen diffusion into the cobalt subsurface. This could have important implications for supported catalysts where high hydrogen exposures (1 + atm) are expected. Future studies investigating the diffusion of hydrogen into the subsurface of nanoparticles could shed an important light on the role of subsurface hydrogen in catalytic cobalt systems, or in systems where treatment by hydrogen is known to induce structural changes.

Conflicts of interest

There are no conflicts to declare.

Acknowledgements

Notes and references

1 J. Wilson and C. De Groot, *J. Phys. Chem.*, 1995, **99**, 7860–7866.

2 J. X. Liu, H. Y. Su, D. P. Sun, B. Y. Zhang and W. X. Li, *J. Am. Chem. Soc.*, 2013, **135**, 16284–16287.

3 Y. Liu and H. Pan, *Hydrogen Storage Materials*, Elsevier B.V., 2013.

4 J. X. Liu, H. Y. Su, D. P. Sun, B. Y. Zhang and W. X. Li, *J. Am. Chem. Soc.*, 2013, **135**, 16284–16287.

5 W. Chen, I. A. W. Filot, R. Pestman and E. J. M. Hensen, *ACS Catal.*, 2017, **7**, 8061–8071.

6 O. R. Inderwildi, S. J. Jenkins and D. A. King, *J. Phys. Chem. C*, 2008, **112**, 1305–1307.

7 R. Tran, Z. Xu, B. Radhakrishan, D. Winston, W. Sun, K. A. Persson and S. P. Ong, *Sci. Data*, 2016, **3**, 160080.

8 K.-H. Ernst, E. Schwarz and K. Christmann, *J. Chem. Phys.*, 1994, **101**, 5388–5401.

9 Z. Huesges and K. Christmann, *Z. Physiol. Chem.*, 2013, **227**, 881–899.

10 P. Van Helden, J. A. Van Den Berg and C. J. Weststrate, *ACS Catal.*, 2012, **2**, 1097–1107.

11 C. J. Weststrate, M. Mahmoodinia, M. H. Farstad, I. H. Svenum, M. D. Strømsheim, J. W. Niemantsverdriet and H. J. Venvik, *Catal. Today*, 2019, 0–1.

12 A. L. Cabrera, *J. Vac. Sci. Technol., A*, 1993, **11**, 205–208.

13 R. Duś and W. Lisowski, *Surf. Sci.*, 1976, **61**, 635–645.

14 W. Lisowski, *Appl. Surf. Sci.*, 1989, **37**, 272–282.

15 A. D. Johnson, S. P. Maynard, S. P. Daley, Q. Y. Yang and S. T. Ceyer, *Phys. Rev. Lett.*, 1991, **67**, 927–930.

16 S. T. Ceyer, *Acc. Chem. Res.*, 2001, **34**, 737–744.

17 A. D. Johnson, S. P. Daley, A. L. Utz and S. T. Ceyer, *Science*, 1992, **257**, 223–225.

18 H. Okuyama, W. Siga, N. Takagi, M. Nishijima and T. Aruga, *Surf. Sci.*, 1998, **401**, 344–354.

19 R. J. Behm, V. Penka, M.-G. Cattania, K. Christmann and G. Ertl, *J. Chem. Phys.*, 1983, **78**, 7486–7490.

20 G. E. Gdowski, T. E. Felter and R. H. Stullen, *Surf. Sci.*, 1987, **181**, 147–155.

21 W. Y. Yu, G. M. Mullen and C. B. Mullins, *J. Phys. Chem. C*, 2013, **117**, 19535–19543.

22 H. R. Gray, *NASA Tech. Note TN D-7805*, 1975, 1–43.

23 D. J. Klinke, D. J. Dooling and L. J. Broadbelt, *Surf. Sci.*, 1999, **425**, 334–342.

24 J. Greeley and M. Mavrikakis, *J. Phys. Chem. B*, 2005, **109**, 3460–3471.

25 G. Kresse and J. Hafner, *Phys. Rev. B: Condens. Matter Mater. Phys.*, 1993, **47**, 558.

26 G. Kresse and J. Hafner, *Phys. Rev. B: Condens. Matter Mater. Phys.*, 1994, **49**, 14251.

27 G. Kresse and J. Furthmiiller, *J. – Am. Water Works Assoc.*, 1996, **6**, 15–50.

28 G. Kresse, J. Furthmüller, Y. J. Li, Y. J. Chen, J. C. Walmsley, R. H. Mathinsen, S. Dumoulin, H. J. Roven, S. Yip, T. Supervisor and S. Chen, *Phys. Rev. B: Condens. Matter Mater. Phys.*, 1996, **54**, 11169–11186.

29 G. Kresse and D. Joubert, *Phys. Rev. B.*, 1999, **59**, 11–19.

30 P. E. Blochl, *Phys. Rev. B: Condens. Matter Mater. Phys.*, 1994, **50**, 17953–17979.

31 J. P. Perdew, K. Burke and M. Ernzerhof, *Phys. Rev. Lett.*, 1996, **77**, 3865–3868.

32 J. P. Perdew, K. Burke and M. Ernzerhof, *Phys. Rev. Lett.*, 1997, **78**, 1396.

33 F. Ono and H. Maeta, *Le J. Phys., Colloq.*, 1988, **49**, C8–63.

34 H. J. Monkhorst and J. D. Pack, *Phys. Rev. B: Condens. Matter Mater. Phys.*, 1976, **13**, 5188–5192.

35 M. Methfessel and A. T. Paxton, *Phys. Rev. B: Condens. Matter Mater. Phys.*, 1989, **40**, 3616–3621.

36 G. Henkelman and H. Jónsson, *J. Chem. Phys.*, 2000, **113**, 9901–9904.

15286 | *Phys. Chem. Chem. Phys.*, 2020, **22**, 15281–15287

This journal is © the Owner Societies 2020

37 P. A. Redhead, *Vacuum*, 1962, **12**, 203–211.

38 D. W. Flaherty, N. T. Hahn, D. Ferrer, T. R. Engstrom, P. L. Tanaka and C. B. Mullins, *J. Phys. Chem. C*, 2009, **113**, 12742–12752.

39 G. Henkelman, A. Arnaldsson and H. Jónsson, *J. Chem. Phys.*, 2006, **124**, 1–9.

40 K. García-Díez, J. Fernández-Fernández, J. A. Alonso and M. J. López, *Phys. Chem. Chem. Phys.*, 2018, **20**, 21163–21176.

41 K. H. Bornscheuer, S. R. Lucas, W. J. Choyke, W. D. Partlow and J. T. Yates, *J. Vac. Sci. Technol., A*, 1993, **11**, 2822–2826.

42 U. Bischler and E. Bertel, *J. Vac. Sci. Technol., A*, 1993, **11**, 458–460.

43 M. Pan, D. W. Flaherty and C. B. Mullins, *J. Phys. Chem. Lett.*, 2011, **2**, 1363–1367.

44 E. A. Lewis, D. Le, C. J. Murphy, A. D. Jewell, M. F. G. Mattera, M. L. Liriano, T. S. Rahman and E. C. H. Sykes, *J. Phys. Chem. C*, 2012, **116**, 25868–25873.

45 B. Hammer, L. B. Hansen and J. K. Nørskov, *Phys. Rev. B: Condens. Matter Mater. Phys.*, 1999, **59**, 7413–7421.

This journal is © the Owner Societies 2020

Phys. Chem. Chem. Phys., 2020, **22**, 15281–15287 | **15287**